Structure and elasticity of composite nanoparticle/polymer nanoshells (hybridosomes®)

Flavien Sciortino, M. Thivolle, Myrtil L. Kahn, C. Gaillard, Soizic Chevance, Fabienne Gauffre

Structure and elasticity of composite nanoparticle/polymer nanoshells (hybridosomes®)

F. Sciortino,[a] M. Thivolle,[a] M. L. Kahn,[b] C. Gaillard,[c] S. Chevance[a] and F. Gauffre*[a]
Author affiliations

* Corresponding authors

[a] Institut des Sciences Chimiques de Rennes, UMR 6226 CNRS, Université Rennes 1, Av. Général Leclerc, 35042 Rennes Cedex, France
E-mail: fabienne.gauffre@univ-rennes1.fr

[b] Laboratoire de Chimie de Coordination UPR8241 CNRS, 205 rte de Narbonne, Toulouse cedex 04, France

[c] INRA, La Géraudière, 44316 Nantes cedex 3, France

Structure and Elasticity of Composite Nanoparticle/Polymer Nanoshells (hybridosome®)

F. Sciortino,[a] M. Thivolle, [a] M. L. Kahn,[b] C. Gaillard,[c] S. Chevance, [a] F. Gauffre[a]

Our group recently introduced a new process to synthesize nanoparticle shells of about 100nm, named "hybridosomes®". Here, the structure and the mechanical properties of hybridosomes® made from iron oxide nanoparticles and poly(acrylic acid) are characterized using TEM, AFM and an osmotic compression technique. For this latter, the size distribution of the hybridosomes is monitored by nanoparticle tracking analysis (NTA) in presence of poly(ethylenglycol)s of different molecular weights. It is found that the size of the hybridosomes® can be tuned from ca 80nm to over 110nm by adjusting the amount of nanoparticles and that their shell consists in a single layer of nanoparticles, with a porous structure. The size of the pores is estimated from osmotic compression experiments at ca 4 000 g mol^{-1}. The mechanical properties are measured both at the ensemble level using size measurements under osmotic pressure and at the single nanoparticle level by Atomic Force Microscopy nanoindentation. Both osmotic and AFM experiments are analyzed in the framework of the continuum elastic theory of thin shells and yield a value of the Young's modulus of the order of the MPa.

A. Introduction

Capsules are abundant in nature where membranes (of cells, nucleus, exosomes…) and shells (of eggs) provide a protective barrier while enabling selective exchange. At the age of modern technology, micro- and nano-capsules (or vesicles) are used as protection shells for enzymes, vessels for drug or gene vectorization, nanoreactors for confined chemical reactions and heterogeneous catalysis, or to template the formation of new materials.[1–3] A lot of efforts has been devoted to the elaboration of submicronic synthetic capsules, each of them having their own advantages and disadvantages. Among them, liposomes, polymersomes and multilayered polyelectrolyte nanocapsules are the most documented.[4–9] More recently, nanoparticle shells have appeared as highly desirable for the elaboration of metamaterials[10–12] as well as for biomedical applications such as imaging and theranostics.[13,14] The methods that have been developed so far to elaborate nanoparticle shells fall into two categories. The first one makes use of amphiphilic block copolymers to direct the self-assembly.[15,16] The second family is based on the use of sacrificial templates, either silica or latex particles over which a layer of nanoparticles is deposited.[6] A calcination step is generally required to remove the templating core.

Recently, our group introduced a simple and robust procedure to elaborate hybrid polymer/nanoparticles capsules (diameter ~ 100 nm), that were coined hybridosomes®.[17] The shell of the capsules is made from inorganic nanoparticles crosslinked by polymers. Interestingly, hybridosomes made from superparamagnetic iron oxide nanoparticles (IONPs) (maghemite) and crosslinked with poly(acrylic acid) (PAA) showed excellent properties as MRI contrast agent and can easily encapsulate hydrophobic compounds. Their bench stability as dispersions was demonstrated to be at least 1 year. In addition, hybridosomes® were prepared from various inorganic nanoparticles including quantum dots, plasmonic and upconverting nanoparticles, the only limitation being that they should be coated by an hydrophobic layer. Thus, these capsules of a new type hold many promises particularly for imaging and theranostic.

Obviously, the shell permeability and mechanical properties of the capsules are of great importance in many aspects such as encapsulation, triggered release, deformation into flow, rheology, and even adhesion. For instance, the protein shells of viruses are extremely rigid and tailored to resist to internal pressure generated by encapsulated genetic material, as high as 10 MPa.[18,19] In contrast, red blood cells are among the less rigid materials, but nevertheless can withstand extreme stretching forces and squeeze into very small capillaries.[20] Both liposomes and polymersomes

membranes are bilayers constituted of phospholipids or amphiphilic block copolymers, respectively. Liposomes are generally characterized by thermal membrane fluctuations and a high lateral mobility due to the low molecular weight (< 1 kDa) of their constituent phospholipids. Polymer membranes are more resistant to rupture, and interestingly the membrane properties of polymersomes can be tailored by a precise molecular design of the constituting blocks.[21,22] There has been also much interest in the investigation of the mechanical properties of multilayered polyelectrolyte nanocapsules, because the thickness of the shell is directly related to the number of layers and can be tuned in a large extent.[23–27]

In this paper, we investigated the structure of the shell and mechanical properties of hybridosomes® made from IONPs and PAA. An osmotic technique, associated with nanoparticle tracking analysis (NTA) was introduced to investigate the effect of isotropic compression. To this aim, hybridosomes® were suspended into solutions of poly(ethylenglycol) (PEG) of various size, and the size distribution of the capsules was measured. This technique also enables to determine the porosity of the shell, since low molecular weight PEGs obviously equilibrate between the interior and the exterior of the capsules. In complement to osmotic pressure experiments, the effect of local stress was investigated using the Atomic Force Microscopy (AFM) nanoindentation technique. The results were interpreted using the theory of thin shell elasticity to determine the Young's modulus of the composite shell. The compositions in polymer and in nanoparticles were both varied, to determine their respective role in hybridosome® size and shell properties.

B. Experimental

Materials: Octylamine was purchased from Sigma–Aldrich and stored as received in an argon-filled glove box. $\{Fe[N(SiMe_3)_2]_2\}$ (purchased from Nanomeps) was stored as received in the fridge of the glove box. Tetrahydrofuran (VWR) was used as received. Poly(acrylic acid) PAA (450 000 g mol^{-1}) was purchased from Aldrich.

Nanoparticle synthesis: The synthesis of the maghemite (γ-Fe_2O_3) IONPs was achieved *via* hydrolysis of an organometallic Fe(II) precursor following a recently reported procedure.[40] The reaction was achieved in pure octylamine and in mild conditions of pressure and temperature. Water was deoxygenated by bubbling argon 30 mins before the reaction and stored under argon. The precursor $\{Fe[N(SiMe_3)]_2\}$ and octylamine (2 eq. to the precursor) were introduced in vials in a glovebox under argon. After a dark homogeneous liquid was obtained the vials were placed in a closed reactor, removed from the glovebox, and set to 40°C. After 15 min, H_2O (2.1 eq.) was introduced in the reactor. The reaction was stopped after 3 days by placing the reactor under vacuum. The mixture was then exposed to air and dispersed in THF. The solution was then centrifuged at 19 000 rcf for 10 min and the pellet discarded. After air oxidation, superparamagnetic magnetite nanocrystals with a mean diameter d= 5.5 nm and a narrow size distribution (standard deviation 1.0 nm) are obtained.

Preparation of stock dispersions of hybridosomes. The hybridosomes were prepared by adding water to a THF solution containing the IONPs, in order to reach a water volume fraction of 0.8, promptly followed by vortexing. After ca 15 h, PAA was added to the mixture as a concentrated aqueous solution. The THF was then totally removed by slow evaporation (15h at 40°C), after which the remaining volume was ca 500 µL. It was verified that after this treatment, no traces of THF could be detected by ^{1}H NMR.

Nanoparticle Tracking Analysis: Stock suspensions of hybridosomes were diluted 100 times prior to NTA measurements. For each samples, 3 acquisitions with acquisition times of 60 s were performed. The relative standard deviation is calculated from SD*100/mean.

Osmotic compression*:* 5 µL of the stock dispersion were first diluted into water and then mixed with an appropriate volume of PEG aqueous, and of 200 nm calibrated latex solution to reach a final volume 500µL and the desired PEG concentration. Determination of the osmotic pressure from PEG concentration. At very low PEG concentration, the osmotic pressure (*P*) can be derived from the molar concentration (*C*) using the law

of ideal gas *P= RTC*. However, one should be careful to take into account the divergence from ideality at higher concentrations.[41] The conversion from molarity to osmotic pressure was extrapolated from experimental data by Money (PEG 1K, 4K, 10K)[41] and Shaykewich (PEG 20 K).[42]

Transmission Electron Microscopy: A drop of 40 µl was first placed on a carbon-coated TEM copper grid (Quantifoil, Germany). The sample was then negatively stained with 2 % w/w uranyl acetate (Merck, Germany) previously filtered on a 0.2 µm filter unit. The grid was then air-dried before introducing it in the electron microscope. The samples were viewed using a JEM 1230 'Cryo' microscope (JEOL, Japan) operated at 80 kV and equipped with a LaB6 filament. All the micrographs were recorded on a Gatan 1.35 K x 1,04 K x 12 bit ES500W CCD camera.

Atomic Force Microscopy: Samples were imaged in fluid over an area of 500 nm^2 to 20 μm^2 at 0.2 to 0.5 Hz operated in the Peak Force Tapping mode on a BioScope Catalyst AFM (Bruker AXS, Santa Barbara, CA) using a small volume liquid cell and a set-point varying from 4 nN to 115 nN according to the strength applied in order to progressively crushing the particles. SCANASIST-Fluid AFM tips (Bruker AFM Probes, Camarillo, CA) with a nominal spring constant, resonant frequency and radius of 1.5 N m^{-1}, 150 kHz and 20 nm, respectively, were used for each experiments. Thermal noise method was systematically used to refine the spring constant value of the cantilevers. Force spectroscopy curves were acquired in water by approaching a tip onto the sample at a pulling speed of 1 µm s^{-1}. Sensitivity calibration was determined in water solution over a piece of freshly silicon substrate at room temperature (25 °C). Force curves were taken at different locations on the particles, in order to account for any heterogeneity in the coverage of the surface. Force measurements were acquired from around 500 different points at the surface. AFM data were analyzed using the Nanoscope Analysis 1.5 software (Bruker AXS, Santa Barbara, CA) to extract the effective Young's modulus as the slope of the linear elastic region of the approach-retract curves.

C. Results and discussion

All details about the synthesis of the hybridosomes® were described previously.[17] Briefly, the process consists in three steps (**Figure 1**). First, liquid droplets are coated with the hydrophobic nanoparticles in a water/THF (80:20) mixture forming the primary nanoparticle shell (Step 1). Then, the nanoparticle shell is crosslinked by a coordinating polymer (Step 2). Finally, the solvent is removed by evaporation, yielding the hybrisomes® with an aqueous core, and the samples are purified by magnetic separation (Step 3). All the hybridosomes® used in this study were prepared from iron oxide nanoparticles (IONP; 5.5 nm ± 1nm) crosslinked with poly(acrylic acid) (PAA 450 000 g mol^{-1}). TEM analysis of hybridosomes® after negative staining occasionally show some open structures (urns, Figure 1). From such pictures, it is clear that the shell is only a few nanometers thick, which is consistent with a single layer of particles. For the following discussion we will consider that the shell thickness (h) is equivalent to the diameter of the IONPs (h ≈ 5nm).

We investigated the influence of the composition of the hybridosomes® (amount of IONPs and of PAA) over their structure. First, we varied the amount of IONPs introduced. **Figure 2a** shows the size histograms for iron concentration in the range 0-25 µg L^{-1} and for a given concentration in polymer ([AA] = 2.25mM) determined by NTA. NTA tracks individual trajectories,

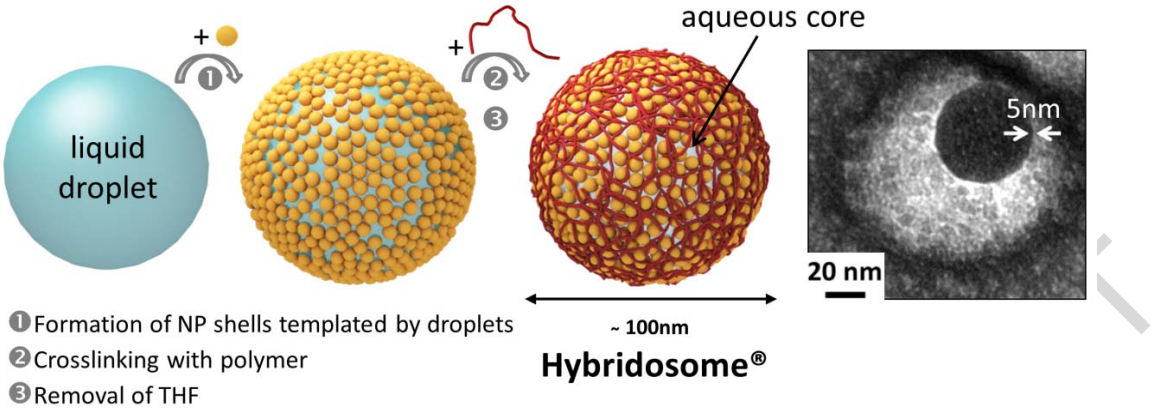

Fig. 1. Process of elaboration of the hybridosomes and TEM observation with negative staining, showing an "open" hybridosome. ([AA]=2.25 mM; [Fe]=12.5 µg mL^{-1})

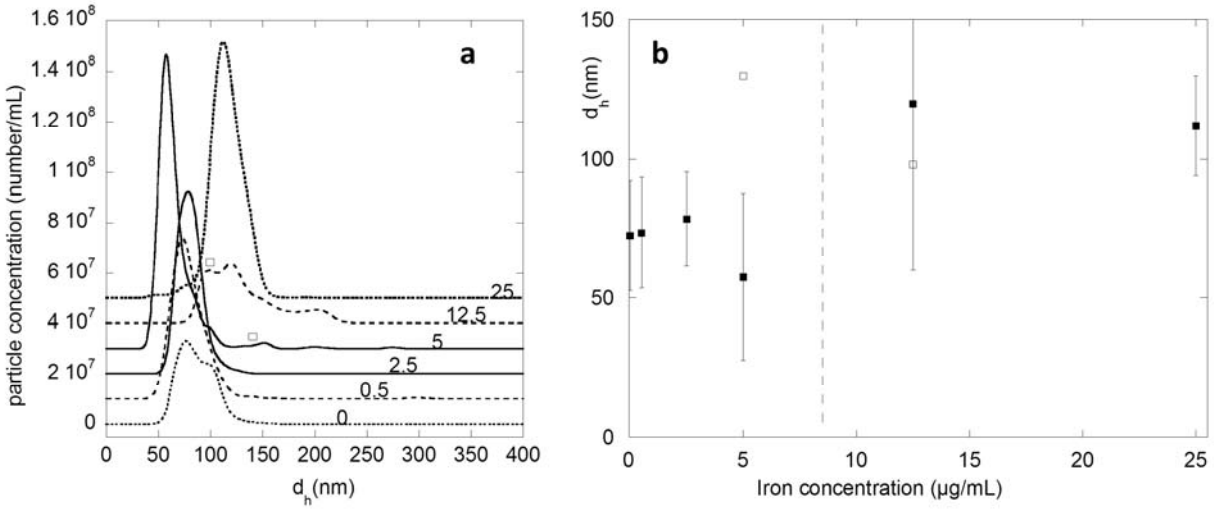

Fig. 2. Influence of the amount of SPION over the size distributions (hydrodynamic diameter d_h) of hybridosomes. (a) Size histograms determined by NTA. The symbol ☐ points out a secondary mode. (b) Main mode (■) and secondary mode (☐) of the distribution. Error bars represent the standard deviation (SD) of the distribution. Concentrations of stock solutions: [Fe]=0;0.5;2.5;5;12.5; 25µg mL^{-1} as indicated on graph; [AA]=2.25mM.

allowing calculation of the diffusion coefficient and thus the hydrodynamic diameter (d_h) of each particle. Reporting the main mode (and when present a secondary mode) *vs* the iron concentration evidences two regimes (Figure 2b). The low concentration regime is characterized by a hydrodynamic diameter (d_h) of ca 80 nm or lower, whereas in the higher concentration regime d_h is over 110 nm. Note that at the transition between the two regimes, coexistence of the two populations is observed. It is common to report the width of the distribution obtained by NTA as the Relative Standard Deviation (RSD, see Experimental Section for details). The histograms are of moderate width (RSD = 17-25%) except in the vicinity of the

transition where the distributions can be considered as polydisperse (RSD ~ 40%), as a result of the coexistence of the two populations. Interestingly, it was also possible to form capsules from PAA only, without the use of nanoparticles. In contrast, varying the amount of PAA to form the hybridosomes® does not significantly change the measured diameter (**Figure 3**), but the distribution widens significantly at lower amounts of PAA and the total amount of capsules decreases. To summarize, the IONPs hybridosomes® can adopt two possible equilibrium conformations, a small size (d_h~ 80 nm) and a larger size (d_h~ 110 nm), at low and high particle concentration, respectively. In the low concentration regime, the size is obviously determined from the polymer properties, whereas in the large concentration regime it is influenced by the presence of the particles. Note that the presence of a population of relatively small size is important for future imaging and theranostic applications, since body clearance of circulating particles increases with particle size.[28]

Two types of experiments were performed to investigate the shell properties of the hybridosomes®. The first type consists in applying an osmotic pressure and the second type a localized force, by nano-indentation. Concerning the osmotic compression, we reasoned that hybridosomes® dispersed in a polymer solution would experience an inward osmotic pressure if the polymer does not diffuse across the shell. In a first set of experiments, PEGs of four molecular masses: 1000 g mol^{-1}; 4000 g mol^{-1}; 10 000 g mol^{-1} and 20 000 g mol^{-1} (marked as 1K, 2K, 10K and 20K, respectively) were used, at increasing concentrations (15; 45; 75 and 100 g L^{-1}). The size distribution of hybridosomes® submitted to the osmotic pressure was analyzed using NTA and renormalized from viscosity effects using a 200 nm calibrated latex (**Figure 4a**). Two facts are remarkable. The first one is that the influence of the shortest PEGs over the size distribution of the hybridosomes® is negligible (PEG 1k) or weak (PEG 4k), whereas a significant amount of shrinking is observed for PEG 10K and 20K. These results evidence the porous nature of the shell, with and estimated molecular cut-off at approximately 4000 g mol^{-1}, or 2 nm in terms of hydrodynamic radius.[29] Thus, PEGs smaller than 4k diffuse across the shell, equilibrating inner and outer osmotic pressures. The second observation is a sharp transition from a monomodal to a multimodal distribution with measured sizes spanning down to 25 nm (which is the detection limit of NTA) at the highest concentrations for PEG 10K and PEG 20K. We interpret this result as a transition between a regime of isotropic compression and a buckling instability, leading to the formation of wrinkles or possibly of inverted hemispheres, as was previously observed for polyelectrolyte vesicles.[23,25,30] It is worthwhile to note that at 0.1 MPa and above, a population of hybridosomes® with a broken shell can be distinguished by the absence of shrinking (indicated by the symbol (*) on Figure 4d). Figure 4e shows the measured hydrodynamic diameter in function of the osmotic pressure, when a main mode can be clearly identified. We estimate the onset of the symmetry breaking instability at a critical pressure P_c=0.075 MPa (materialized by the dotted line) and a critical radius R_c= 95/2= 47.5 nm.

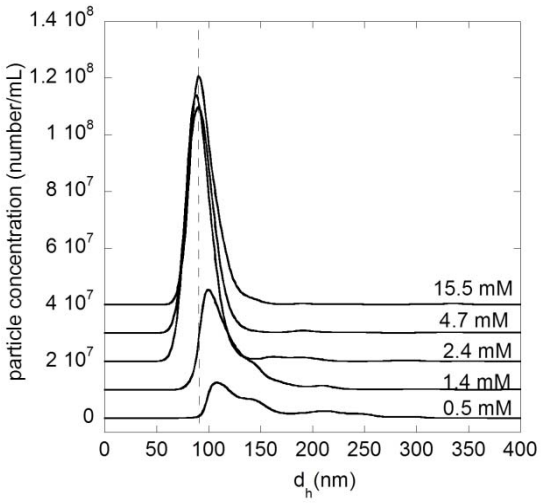

Fig. 3. Influence of the amount of PAA over the size distributions (hydrodynamic diameter dh) of hybridosomes measured by NTA. Concentrations of stock solutions: [Fe]=12.5µg ml-1; [AA]=0.5; 1.4; 2.4; 4.7; 15.5mM as indicated on graph.

Can deformed hybridosomes recover their initial shape if the pressure is relaxed? To address this issue, we took advantage of the magnetic behavior of the IONPs

hybridosomes®. Thus, these latter were separated from the PEG solution using a permanent magnet. After 2 steps of separation and washing with plain water, the hybridosomes® were incubated for 1 hour at 35°C and the size distribution was measured again (**Figure S1**). A large fraction of the deflated shells swell back to their initial size. In addition, a larger population is observed, reflecting the presence of aggregates. Observation of the scattered light during NTA acquisition clearly shows some aggregates in the form of straight chains of a few hybridosomes. Such anisotropic aggregation most probably results from magnetic interactions between hybridosomes. Indeed, hybridosomes exhibit a non-zero magnetic moment in their swollen state (as shown by the fact that they are attracted by a permanent magnet) resulting from coupling between individual IONPs, which is increased under compression because the distance between the IONPs decrease. Interestingly, the compressed hybridosomes do not swell back at room temperature but require some thermal energy to overcome the magnetic interaction.

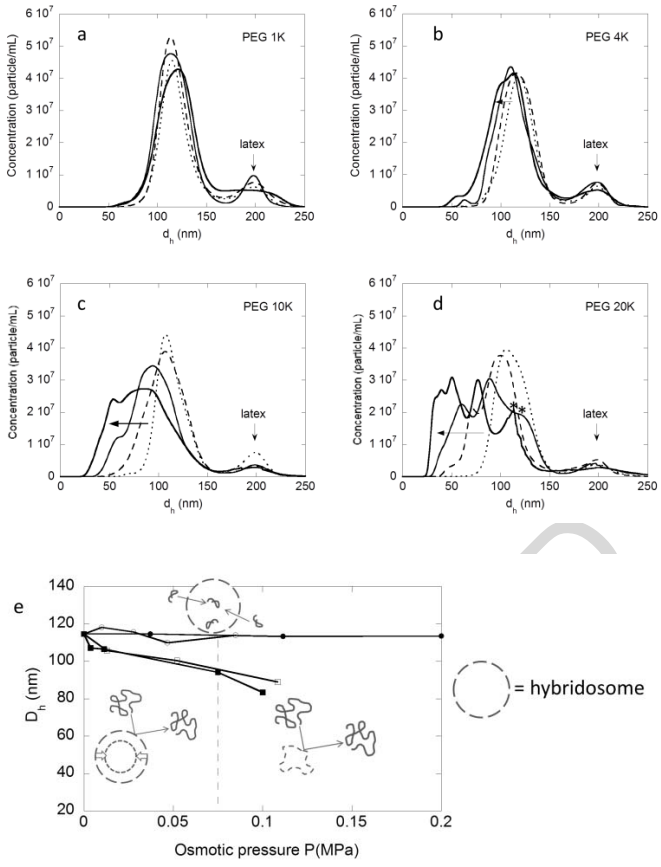

Fig. 4. (a-d) Osmotic compression of hybridosomes dispersed in solutions of PEG 1K, 4K, 10K, 20K. A 200nm latex was added to the dispersion for renormalization of the viscosity. Symbols (*) indicates broken hybridosomes. The PEG concentrations are (···) 15 g L^{-1};(---) 45 g L^{-1}; (—)75 g L^{-1}; (⟶)100 g L^{-1}. (e) Evolution of the size (main mode) of the hybridosomes as a function of osmotic pressure for the 4 sizes of PEG. The dotted line shows the onset of buckling. Hybridosomes: [Fe]= 25 µg mL^{-1}; [AA]=2.25mM.

Our results can be interpreted in the framework of the continuum theory of thin spherical shells. The shell will be regarded as a homogeneous body (which is obviously not the case at the microscopic scale), characterized by a Young modulus (E) and a Poisson ratio (σ). In contrast to lipid vesicles where shear is dominant, polymer vesicles are rather prone to bend (out-of-plane deformations) and stretch (in-plane deformations).[24,31] Let's first examine the case of an isotropic constraint, for instance the evaporation of a solvent core or osmotic compression.[28]

The isotropic compression (or alternatively stretching) of an isotropic hollow shell obeys:[32]

$$R_0 - R = \frac{1-\sigma}{2Eh} P R^2 \qquad \text{(Equation 1)}$$

Compression is costly and the shell is rapidly forced to give up its spherical symmetry to adapt to this new constraint at a lower energy cost.[33] At the onset of instability, the relation between the critical pressure (P_c) and the radius (R_c) is:[32]

$$P_c = \frac{2E}{\sqrt{3(1-\sigma^2)}} \left(\frac{h}{R_c}\right)^2 \qquad \text{(Equation 2)}$$

The main consequence of considering the shell as a continuum is that no other length scale than h and R enter the models. Therefore, Equations 1 and 2 apply at all scales from viruses to ping-pong balls and buildings. It was used previously to determine the

mechanical properties of polyelectrolyte capsules.[23,25,34] Most previous reports on polyelectrolyte capsules monitor shape changes by optical microscopy and analyze the fraction of deformed capsules in function of the osmotic pressure, but were unable to characterize the evolution of the capsule radius with pressure in the subcritical regime, due to high dispersity in size.[24] Remarkably in our case, the narrow dispersity of hybridosomes® enables to follow shrinking during isotropic osmotic compression. Therefore, both the regime of isotropic compression and the onset of instability can be exploited using Equations 1 and 2, respectively. The values h= 5 nm and R_0= 56.5 nm were taken as fixed geometrical parameters in both models. The Poisson ratio is an unknown parameter generally ranging from 0.25 to 0.45. We combined Equations 1 and 2 to evaluate E using arbitrary values of σ in the range 0.25-0.45. Our results were analyzed firstly in the subcritical regime using Equation 1. We fitted pressure *vs* equilibrium radius during isotropic compression (**Figure S2**). Then, using the estimated values of the critical pressure and radius (P_c= 0.075 MPa and R_c= 47.5 nm, **Figure 4e**) Equation 2 gives an independent determination of E. The results show that the value of the Poisson coefficient has in fact little influence (less than 1MPa) over the determination of E. Therefore we arbitrarily used the value σ = 0.3, which yielded E= 1.3 MPa and E= 5.6 MPa using Equation 1 and Equation 2, respectively. Note that these values are one to two orders of magnitude lower than these commonly reported for polyelectrolytes capsules,[23,24] which is consistent with a weaker interaction between IONPs and PAA, than between layers of oppositely charged polyelectrolytes. Thus, hybridosomes® show a relative ability to shrink and swell, that might be exploited for encapsulation and release applications. Despite all our efforts, we were unfortunately unable to image the hybridosomes® under osmotic compression, neither by TEM nor by liquid Atomic Force Microscopy, due to high concentration of PEGs. However, the progressive flattening of the hybridosomes® was imaged by AFM in liquid, by applying a force of increasing intensity over their surface (**Figure S3**).

In contrast to osmotic compression experiments which are at the ensemble level, nanoindentation enables to probe the elasticity of the shell by applying a localized force on a single hybridosome®. Nanoindentation was investigated using AFM keeping an aqueous environment (pure water). In a first set of experiments, force-displacement (FZ) curves measurements were acquired in water by approaching a tip toward the sample at a speed of 1 µm s^{-1} (**Figure 5**). The relative indentation extends to 10 % of the diameter and forces up to 7 nN. FZ curves were taken from around 500 different locations at the surface in order to account for any heterogeneity, and yielded similar results with a standard deviation of ~ 25 %. No alteration of the vesicle was observed after 500 measurements. The approach curves are mostly linear after build up (Figure 5, inset) and retract curves clearly show hysteresis

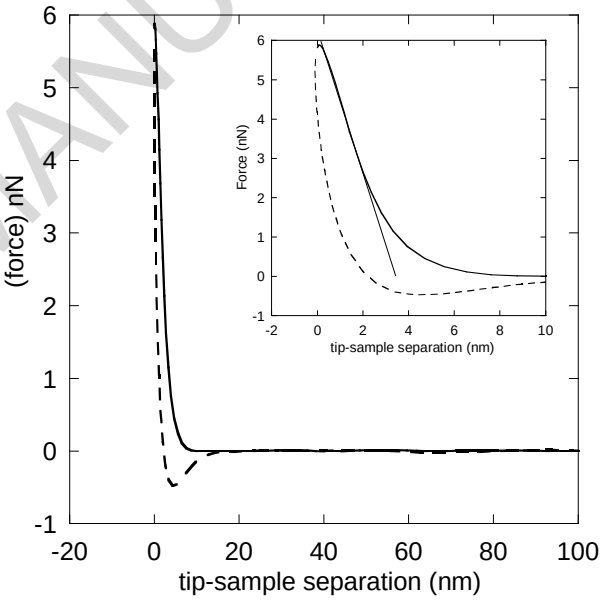

Fig. 5. Typical AFM force-distance approach (—) and retract (--) curve in aqueous solution. Hybridosome: [Fe]= 25 µg mL^{-1}; [AA]=2.25 mM, initial radius 39 nm. The estimated slope from the linear part of the approach curve is 1.8 N m^{-1} (insert).

owing to a viscous and plastic behavior of the nanoparticle surface. We assume that the dynamics of water diffusion across the membrane is fast enough to ensure equilibrium of internal and external pressures.

To analyze the indentation data, we assume that the vesicle remains in a regime of small deformation without developing a buckling instability. This seems reasonable since the maximal displacement (~8 nm) is less than twice the shell thickness. In addition, buckling is characterized by a sudden drop in the measured force, which was not observed here.[18,24] The Young's modulus for the shell can be extracted from the linear slopes of the forward curve in the linear regime using :[35–37]

$$F = \frac{4}{\sqrt{3(1-\sigma^2)}} \frac{\delta E h^2}{R}$$

(Equation 3),

where δ stands for the displacement of the surface. Using Equation 3 to fit the linear part of the forward FZ curve, we find E=1.2 MPa, which again falls in the range of the values determined by osmotic pressure measurements. This value reflects a relatively low degree of interactions between the PAA polymer chains (*via* hydrogen bonding) and between the polymer and the particles (*via* interaction between iron oxide surface and the particles). In comparison, the Young's modulus of multilayered polyelectrolyte capsules is over 100 MPa at room temperature, where they are in a glassy state, but decreases to the MPa beyond the glass-melt transition (typically above 35°C).[37]

It is interesting to note that, due to their relatively low Young's modulus, the hybridosomes® can withstand a certain amount of isotropic compression before buckling, making the elastic deformation domain experimentally observable, in contrast to most vesicular systems reported in the literature. It was reported that hollow thin shells buckle into a variety of complex conformations, including reversed spherical shell and crumpled spheres.[23,38,39] In the present case it is difficult to characterize the shape of the hybridosomes® under pressure because of their small size.

In the following, we investigate the effect of hybridosome composition (amount of IONPs and of PAA) on their elastic properties. In a first set of experiments, the effect of osmotic pressure was compared for two samples with different amount of IONPs (12.5 µg mL^{-1} and 25 µg mL^{-1}). **Figure S4** shows that both samples have similar properties in terms of porosity and critical pressure. As mentioned previously, during their elaboration, the hybridosomes® prepared with relatively low amount of particles contract on removal of the solvent until close contact of the IONPs. This explains both the lower mean size of the sample with [Fe]=12.5 µg mL^{-1} compared to that with [Fe]=25 µg mL^{-1}, and the absence of significant effect of IONPs on the mechanical properties. In a second set of experiments, hybridosomes® with various contents of PAA were prepared in the range 0.5-15 mM. PEG 10K was selected for osmotic compression, assuming that it will not penetrate through the shells of hybridosomes®. **Figure 6** demonstrates that, at low PAA content ([AA]=0.4 and 1.4mM), a mechanical instability

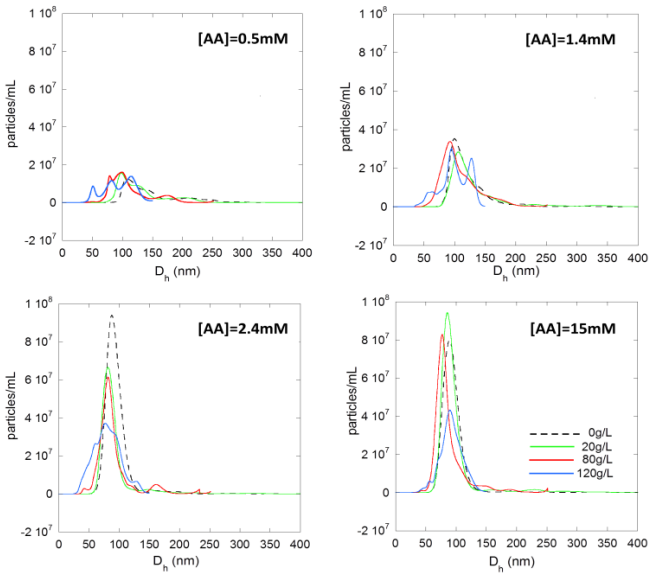

Fig. 6. Effect of osmotic compression for hybridosomes prepared with [Fe]= 12.5 µg mL^{-1} and different amounts of PAA (Concentration in terms of AA units). Compression with PEG 10K at (—)0; (---) 20; (- - -) 80; (···) 120 g L^{-1}. Concentrations of PAA as indicated on graphs.

develops and the hybridosomes® deform under osmotic pressure. This is consistent with the hypothesis that PEG 10K is prevented from diffusing across the shell. The shell of hybridosomes® prepared with larger

amounts of PAA should be even more impermeable to PEG 10K. Therefore, an osmotic pressure difference is exerted on the shell for all samples in the investigated range. Interestingly, we observe that increasing PAA contents provides improved mechanical stability under osmotic pressure. At the highest PAA concentration (15.5 mM), hybridosomes® are resistant to deformation exceeding 0.18 MPa (corresponding to 120 g L^{-1} of PEG 10K).

In summary these results show that the mechanical properties of the hybridosomes® are primarily dependent on the content of polymer in the composite shell. Increasing the amount of polymer enables to prepare hybridosomes® with improved mechanical stiffness.

Conclusions

Our result shows that hybridosomes® have a unique shell structure made of a single layer of nanoparticles, crosslinked with a polymer. In the present case, the thickness of the shell was estimated to ca 5 nm, which corresponds to the size of the individual iron oxide nanoparticles. In addition to conventional TEM and AFM analysis, we achieved mechanical measurements using NTA under osmotic pressure. This is to our knowledge, the first report of mechanical measurements at the ensemble level of submicronic vesicular structures. Osmotic compression experiments demonstrated that this shell is porous, enabling size selection of solute with a MWCO of ca 4 kDa, which may be further used to protect encapsulated compounds from enzymatic degradation. The experimental results were interpreted in the framework of the continuum thin shell theory. It was found that the hybridosomes® have a soft deformable shell, with a Young's modulus of the order of the MPa, which explains their oustanding mechanical properties, such as long term stability, easy deformation and shape recovery. In addition, the hybridosomes® size and their shell properties can be tuned by varying their composition. These features are highly valuable for future biomedical applications, as contrast agent and drug carriers, to withstand high osmotic pressure in blood vessels and squeeze into small capillaries. The mechanical deformations of hybridosomes® made from IONPS should induce changes in their response to magnetic field, which is important for imaging (MRI) and sensing applications. This will be investigated in further studies.

Acknowledgements

This work was supported by the French Ministry of Education and Research (F. Sciortino's grant) and the CNRS. F.G. thanks warmly I. Cantat and B. Dollet for fruitful discussions around the book of Landau and Lifshitz and a hot chocolate. .

Notes and references

1 C. G. Palivan, R. Goers, A. Najer, X. Zhang, A. Car and W. Meier, *Chem. Soc. Rev.*, 2016, **45**, 377–411.

2 L. Schoonen and J. C. M. van Hest, *Adv. Mater.*, 2016, **28**, 1109–1128.

3 J. Hu, M. Chen, X. Fang and L. Wu, *Chem. Soc. Rev.*, 2011, **40**, 5472.

4 W. Meier, *Chem. Soc. Rev.*, 2000, **29**, 295–303.

5 A. Akbarzadeh, R. Rezaei-Sadabady, S. Davaran, S. W. Joo, N. Zarghami, Y. Hanifehpour, M. Samiei, M. Kouhi and K. Nejati-Koshki, *Nanoscale Res. Lett.*, 2013, **8**, 102.

6 M. Björnmalm, J. Cui, N. Bertleff-Zieschang, D. Song, M. Faria, M. A. Rahim and F. Caruso, *Chem. Mater.*, 2017, **29**, 289–306.

7 J. Gaitzsch, X. Huang and B. Voit, *Chem. Rev.*, 2016, **116**, 1053–1093.

8 A. M. Carmona-Ribeiro, *Chem. Soc. Rev.*, 1992, **21**, 209–214.

9 C. S. Peyratout and L. Dähne, *Angew. Chem. Int. Ed.*, 2004, **43**, 3762–3783.

10 A. Baron, A. Aradian, V. Ponsinet and P. Barois, *Opt. Laser Technol.*, 2016, **82**, 94–100.

11 S. Gomez-Graña, A. Le Beulze, M. Treguer-Delapierre, S. Mornet, E. Duguet, E. Grana, E. Cloutet, G. Hadziioannou, J. Leng, J.-B. Salmon, V. G. Kravets, A. N. Grigorenko, N. A. Peyyety, V. Ponsinet, P. Richetti, A. Baron, D. Torrent and P. Barois, *Mater Horiz*, 2016, **3**, 596–601.

12 L. Malassis, P. Massé, M. Tréguer-Delapierre, S. Mornet, P. Weisbecker, P. Barois, C. R. Simovski, V. G. Kravets and A. N. Grigorenko, *Adv. Mater.*, 2014, **26**, 324–330.

13 Y. Liu, J. He, K. Yang, C. Yi, Y. Liu, L. Nie, N. M. Khashab, X. Chen and Z. Nie, *Angew. Chem. Int. Ed.*, 2015, **54**, 15809–15812.

14 J. Song, P. Huang and X. Chen, *Nat Protoc.*, 2016, **11**, 2287–2299.

15 R. Chen, D. J. G. Pearce, S. Fortuna, D. L. Cheung and S. A. F. Bon, *J. Am. Chem. Soc.*, 2011, **133**, 2151–2153.

16 S. Lecommandoux, O. Sandre, F. Chécot, J. Rodriguez-Hernandez and R. Perzynski, *Adv. Mater.*, 2005, **17**, 712–718.

17 F. Sciortino, G. Casterou, P.-A. Eliat, M.-B. Troadec, C. Gaillard, S. Chevance, M. L. Kahn and F. Gauffre, *ChemNanoMat*, 2016, **2**, 796–799.
18 J. P. Michel, I. L. Ivanovska, M. M. Gibbons, W. S. Klug, C. M. Knobler, G. J. L. Wuite and C. F. Schmidt, *Proc. Natl. Acad. Sci.*, 2006, **103**, 6184–6189.
19 R. Zandi and D. Reguera, *Phys. Rev. E*, 2005, **72**.
20 P. R. Zarda, S. Chien and R. Skalak, *J. Biomech.*, 1977, **10**, 211–221.
21 J.-F. Le Meins, O. Sandre and S. Lecommandoux, *Eur. Phys. J. E*, 2011, **34**, 14.
22 B. M. Discher, H. Bermudez, D. A. Hammer, D. E. Discher, Y.-Y. Won and F. S. Bates, *J. Phys. Chem. B*, 2002, **106**, 2848–2854.
23 C. Gao, E. Donath, S. Moya, V. Dudnik and H. Möhwald, *Eur. Phys. J. E*, 2001, **5**, 21–27.
24 F. Dubreuil, N. Elsner and A. Fery, *Eur. Phys. J. E - Soft Matter*, 2003, **12**, 215–221.
25 V. V. Lulevich, D. Andrienko and O. I. Vinogradova, *J. Chem. Phys.*, 2004, **120**, 3822–3826.
26 V. V. Lulevich, S. Nordschild and O. I. Vinogradova, *Macromolecules*, 2004, **37**, 7736–7741.
27 H. Bermudez, A. K. Brannan, D. A. Hammer, F. S. Bates and D. E. Discher, *Macromolecules*, 2002, **35**, 8203–8208.
28 M. Longmire, P. L. Choyke and H. Kobayashi, *Nanomed.*, 2008, **3**, 703–717.
29 J. K. Armstrong, R. B. Wenby, H. J. Meiselman and T. C. Fisher, *Biophys. J.*, 2004, **87**, 4259–4270.
30 G. A. Vliegenthart and G. Gompper, *New J. Phys.*, 2011, **13**, 045020.
31 Z. C. Tu and Z. C. Ou-Yang, *Phys. Rev. E*, 2003, **68**.
32 L.D. Landau and E.M. Lifshitz, in *Course of Theoretical Physics*, Butterworth-Heinemann, Oxford, 3rd edn., 1997, vol. 7.
33 E. Helfer, S. Harlepp, L. Bourdieu, J. Robert, F. C. MacKintosh and D. Chatenay, *Phys. Rev. Lett.*, 2001, **87**.
34 C. Gao, S. Leporatti, S. Moya, E. Donath and H. Möhwald, *Langmuir*, 2001, **17**, 3491–3495.
35 B. Audoly and Y. Pomeau, in *Elasticity and Geometry*, Oxford University Press, 2010.
36 A. Fery and R. Weinkamer, *Polymer*, 2007, **48**, 7221–7235.
37 R. Mueller, K. Köhler, R. Weinkamer, G. Sukhorukov and A. Fery, *Macromolecules*, 2005, **38**, 9766–9771.
38 C. I. Zoldesi, C. A. van Walree and A. Imhof, *Langmuir*, 2006, **22**, 4343–4352.
39 F. Quemeneur, C. Quilliet, M. Faivre, A. Viallat and B. Pépin-Donat, *Phys. Rev. Lett.*, 2012, **108**, 108303.
40 G. Casterou, V. Collière, P. Lecante, Y. Coppel, P.-A. Eliat, F. Gauffre and M. L. Kahn, *Chem. Eur. J.*, 2015, **21**, 18855–18861.
41 N. P. Money, *Plant Physiol.*, 1989, **91**, 766–769.
42 J. Williams and C. F. Shaykewich, *Can. J. Soil Sci.*, 1969, **49**, 397–401.